Journal of Polymer Science

WILEY

JOURNAL OF POLYMER SCIENCE

RESEARCH ARTICLE OPEN ACCESS

Active Learning-Driven Inverse Design of Polyurethane Foams for EV Battery Applications

Michael Hoffmann | Sudarsan M. Pai | Rodrigo Q. Albuquerque | Simon Kastl | Holger Ruckdäschel

University of Bayreuth, Bayreuth, Germany

Correspondence: Holger Ruckdäschel (ruckdaeschel@uni-bayreuth.de)

Received: 3 March 2025 | **Revised:** 22 May 2025 | **Accepted:** 29 May 2025

Funding: This work was supported by Bayerisches Staatsministerium für Bildung und Kultus, Wissenschaft und Kunst, F.2-M7426.10.2.1/4/16; Deutsche Forschungsgemeinschaft, 437872031 (AL474/45-1).

Keywords: active learning | inverse design | PUR foams | virtual data

ABSTRACT

The rapid evolution of the electric vehicle (EV) industry demands advanced materials for battery protection, with polyurethane (PUR) foams emerging as a promising solution due to their thermal insulation, mechanical adaptability, and fire resistance properties. This study introduces an active learning-driven inverse design (AL-ID) framework, leveraging machine learning (ML) to systematically optimize PUR foam compositions exhibiting desired density and mechanical strength. AL was employed to iteratively refine the ML model by targeting high-uncertainty regions, reducing experimental effort while improving predictive accuracy. Bayesian optimization (BO) further enhanced the search for optimal compositions by balancing exploration and exploitation. The framework demonstrated significant improvements in model performance, with Mean Absolute Error (MAE) and R^2 scores for density and mechanical strength predictions efficiently improving as the dataset grew. Besides successfully selecting 11 good material candidates out of 616,008 virtual compositions, the final ML models have shown small MAE values and good R^2 scores. This study underscores the potential of ML-driven frameworks to accelerate material discovery.

1 | Introduction

The rapid evolution of the electric vehicle (EV) industry necessitates the development of advanced materials capable of ensuring comprehensive protection and high performance for battery systems [1]. Among the various material solutions, polyurethane (PUR) foams, particularly those enhanced with strategically selected fillers, have gained significant attention due to their unique combination of thermal insulation, mechanical adaptability, and critical fire resistance properties [2].

To appreciate the importance of PUR foams in battery systems, it is helpful to briefly consider their broader relevance and formulation challenges. PUR foams are widely used across a variety of industries due to their versatility, cost-effectiveness, and ease of processing. These foams are employed in a range of applications including packaging, automotive, construction, and insulation [3–5]. In particular, PUR foams are valued for their customizable properties such as density, compressive strength, and thermal insulation, making them ideal for various functional roles. The formulation of PUR foams typically involves combining polyisocyanates and polyols in the presence of catalysts, blowing agents, and additives to achieve specific performance characteristics. The ability to modify foam properties by adjusting formulation parameters is one of the key advantages of PUR foams [6].

Within battery systems, PUR foams serve a multifunctional role, being employed in swell pads, battery cover coatings, and compression or crash pads positioned at the periphery of the

Michael Hoffmann and Sudarsan M. Pai are contributed equally to this work.

battery pack. Their specific application is largely determined by the property profile of the material system, where thermal stability, material density, and compression behavior are key governing factors. Notably, the compression behavior of these foams has a direct impact on the aging behavior of battery cells, requiring a tailored adjustment to match the specific battery chemistry [7]. Furthermore, material density directly influences the thermal conductivity of the foam system, making a simultaneous optimization of these parameters essential to achieving the desired mechanical and thermal performance balance.

To further enhance the thermal stability of PUR foams, inorganic fillers or reactive organic precursors can be incorporated [8–10]. However, while these modifications extend the functional capabilities of the material, they also introduce significant formulation challenges. The interaction between filler composition, dispersion characteristics, and chemical reactivity creates a high-dimensional formulation space, where optimizing performance across multiple competing properties becomes increasingly complex. Traditional material development approaches often fall short in effectively navigating this design landscape due to the complex interplay of material parameters and the limited availability of experimental data [11, 12].

This underscores the need for advanced, data-driven methodologies, such as machine learning-based approaches, which enable a systematic exploration and optimization of material formulations for next-generation battery protection materials. Machine learning (ML) has emerged as a powerful tool in materials science, enabling data-driven optimization of complex formulations while reducing experimental effort [13, 14]. Unlike traditional approaches such as design of experiment (DoE), ML algorithms can efficiently identify structure–property relationships, predict material behavior, and dynamically adapt formulations to evolving performance requirements. Bayesian optimization (BO), for instance, has proven effective in accelerating material discovery and enhancing process efficiency [15–22]. This shift toward computationally guided material design has paved the way for inverse design methodologies, which aim to systematically identify optimal material compositions with targeted properties.

ML and BO approaches have been applied to PUR foams for tasks such as prediction, optimization, and performance enhancement [23–26]. In addition, general ML approaches [27, 28] have been used to predict thermal, rheological, mechanical, and failure properties of PUR-based materials. While optimizing formulations for different aims is one possible goal to achieve better materials, growing experimental datasets via AL with relatively few experiments to generate accurate ML models for different aims (e.g., inverse design) is a very sustainable alternative to perform a similar task, especially compared with time-consuming traditional approaches like design of experiments (DoE), random design, and trial-and-error. To the best of our knowledge, no AL investigation on PUR to grow a dataset while monitoring two target properties (the foam density and the force at 30% strain) has been reported in the literature.

The aim of this work is to introduce a novel active learning-driven inverse design (AL-ID) framework tailored for PUR foam development. The proposed methodology aims to sustainably develop novel PUR compositions to prepare foams that simultaneously exhibit desired values of the density and force at desired strain values, which are critical properties for EV battery applications. Starting from a small experimental dataset, different ML models were used to suggest novel formulations based on the uncertainty sampling AL strategy applied to a pool of more than 600,000 different virtual experiments (or compositions). It is shown that the use of complementary ML models in the sequential filtering of the virtual compositional space is able to efficiently screen the large virtual space to search for optimal experiments. This study demonstrates the effectiveness of the AL-ID approach in overcoming traditional material design limitations, as described in the next sections.

2 | Methodology

2.1 | Experimental Trials

The investigated material formulations were based on the fundamental components polyisocyanate (A), polyol (B), and polysilazane (C). For the polyisocyanate component (A), a combination of aliphatic (Desmodur N31100) and aromatic (Desmodur VL) polyisocyanates in a 50:50 ratio was utilized (both supplied by Covestro AG, Germany). The polyol component (B) consisted of a reactive polyether polyol (Hyperlite 1674, Covestro AG, Germany). For component C, the polysilazane precursor Durazane 1800 (Merck KGaA, Germany) was employed. 1,4-Butanediol and glycerol were used as chain extenders and crosslinking agents. Demineralized water served as a blowing agent to achieve the desired porosity. As a filler, a milled and surface-treated silica (AMOSIL FW600 KST) was incorporated, which was kindly provided by Quarzwerke–HPF Minerals (Frechen, Germany). Additionally, a particulate flame retardant (FR, Exolit AP422) from Clariant AG (Muttenz, Switzerland) was utilized. The key material properties of the employed components are summarized in Tables 1 and 2.

2.2 | Sample Preparation

To prepare the material formulations, the additives water, 1,4-butanediol, and glycerol were precisely weighed and incorporated into component B within a plastic container (diameter: 60 mm). The mixture was subsequently homogenized using a speed mixer (DAC 150.1 FVZ, Hauschild & Co. KG, Hamm, Germany) at 3000 rpm for 60 s to ensure uniform dispersion. Following this, the fillers were incorporated in one or more dispersion cycles, depending on their total amount, with a mixing duration of 90 s at 3000 rpm in the same speed mixer. Once dispersion was complete, the material was cooled to the processing temperature (room temperature or 35°C) to ensure optimal handling and further processing. The distribution of fillers among the components was as follows:

- *Component A*: SiO_2-based filler, where

$$m_{\text{Filler}} \leq 2 \times m_{\text{Component A}}$$

- *Component B*: FR and SiO_2-based filler, where

$$m_{\text{Filler}} \leq 2 \times m_{\text{Component B}}$$

TABLE 1 | Key material properties of the employed components.

Trading name	Type	Equivalent weight [g/eq]	Density [g/cm³]	Functionality	Viscosity [mPa s]
Desmodur VL	pMDI	133	1.23	2.6	90 ± 20
Desmodur N31100	HDI	215	1.10	2.5	550 ± 150
Hyperlite 1674	reactive PPG-Triol	2077	1.02	3	1150 ± 100
Durazane 1800	Organic polysilazane	64.35	1.00	—	25 ± 5
Glycerin	Triol	—	1.26	3	1480
1,4-Butanediol	Diol	—	1.02	2	90

TABLE 2 | Properties of fillers and flame retardants.

Trading name	Density [g/cm³]	Lateral spread D50 [μm]	Surface coating	Surface area [m²/g]
Amosil FW600 KST	2.2	4	Hydrophobic	4.0
Exolit AP422	1.9	17	—	—

$$m_{\text{Filler}} = m_{SiO_2} + m_{\text{FSM}}$$

- *Component C*: SiO_2-based filler, where

$$m_{\text{Filler}} \leq 4 \times m_{\text{Component A}}$$

After the dispersion process was completed, all components were combined, and the entire mixture was homogenized again using a speed mixer (DAC 150.1 FVZ, Hauschild & Co. KG, Hamm, Germany) at 3000 rpm for 30 s to ensure uniform distribution. The final formulation was then stored at room temperature to facilitate foaming and curing for 48 h.

2.3 | Static Compression Tests

To assess the deformation behavior of the foam systems, quasi-static compression tests were performed using a Z050 universal testing machine (Zwick GmbH & Co. KG, Ulm, Germany) equipped with a 10 kN load cell. Cylindrical specimens with a diameter of 60 mm and a thickness of 10 mm were subjected to compression at a constant crosshead speed of 5 mm/min until a strain level of 70% was reached. A preload of 2 N was applied to ensure consistent initial contact. All tests were conducted under standardized climatic conditions (23°C, 50% relative humidity).

The resulting compression curves were analyzed with respect to the required force at 10% strain ($k1$), 20% strain ($k2$), and 30% strain ($k3$) to evaluate the mechanical response of the foam formulations. For each material formulation, three specimens were tested, and the mean values were calculated to ensure statistical reliability.

2.4 | Determination of Foam Density

The density of the foam systems was determined in accordance with DIN EN ISO 845 using six cubic specimens. The density (d) of the samples was calculated using the following equation:

$$d\left[\text{kg}/\text{m}^3\right] = \frac{m}{V} \times 10^6 \quad (1)$$

where m represents the mass of the specimen in grams (g) and V denotes the volume of the specimen in cubic millimeters (mm^3).

2.5 | Virtual Data Generation

To explore the vast compositional space of PUR foams, we generated a large virtual dataset by randomly varying the concentrations of key components (e.g., isocyanates, silazanes, polyols, fillers, and blowing agents). Each component was constrained within experimentally feasible ranges to ensure realistic compositions as shown in Table 3.

The generated compositions were filtered to remove unrealistic or impractical combinations, such as those violating the 1:4 ratio of silazanes to isocyanates or having insufficient filler content (FW600 + APP ≥ 70%). This resulted in a robust virtual dataset for model training.

2.6 | Active Learning Framework

A Gaussian process (GP) model was trained on the filtered virtual dataset to predict key foam properties, such as d and $k1 - k3$. The GP model not only provided predictions but also quantified the uncertainty of each prediction using standard deviation (SD). High-uncertainty regions in the compositional space were identified, as these represent areas where the model lacks confidence due to sparse or noisy data.

To refine the model, targeted experiments were conducted on high-uncertainty compositions. The experimental results were added to the dataset, and the GP model was retrained

TABLE 3 | Component ranges and constraints for virtual data generation.

Component	Range	Step size	Constraints
Isocyanates	1–4 wt.%	0.2 wt.%	Silazane-to-Isocyanate ratio: 1:4
Silazanes	3–8 wt.%	0.2 wt.%	Silazane-to-Isocyanate ratio: 1:4
Polyols	18–25 wt.%	0.5 wt.%	—
Chain extenders	0.3–1.5 wt.%	0.1 wt.%	—
Blowing agents	0.1–0.6 wt.%	0.05 wt.%	—
FW600	25–60 wt.%	2 wt.%	FW600 + APP ≥ 70 wt.%
APP	15–25 wt.%	2 wt.%	FW600 + APP ≥ 70 wt.%

iteratively. This AL approach ensured that the model improved with each iteration, focusing on the most informative data points.

To optimize foam compositions for lower d while maintaining other target properties, we employed BO. BO iteratively suggested new compositions likely to achieve the desired properties, balancing exploration (trying new regions) and exploitation (refining known good regions).

2.7 | Model Screening

To ensure reliable predictions, the dataset was expanded before proceeding with model selection. A comprehensive model screening process was conducted using four-fold cross-validation to evaluate model performance. This technique involves partitioning the dataset into four subsets, training the model on three subsets while testing it on the remaining one. The process is repeated four times, with each subset serving as the test set once. Cross-validation helps mitigate overfitting and provides a more robust estimate of model performance, particularly for small datasets.

The models considered in this study included random forest (RF), least absolute shrinkage and selection operator (LASSO), linear regression (LR), kernel ridge regression (KRR), gaussian process regression (GPR), decision tree (DT), extreme gradient boosting (XGBoost), gamma regression (Gamma), bagging regressor (Bagging), support vector regression (SVR), and gradient boosting regressor (GBR). The predictive accuracy of each model was assessed using mean absolute error (MAE) and the coefficient of determination (R^2). The model demonstrating the lowest MAE and highest R^2 for each target property was selected as the optimal model. This selected model was subsequently used in the inverse design phase to suggest experimental conditions that achieve the desired target properties.

2.8 | Inverse Design for Target Properties

Once the GP model was trained sufficiently, it was used for the inverse design to identify optimal foam compositions that achieve specific d values. After further growing the dataset, the following *sequential filtering* approach was employed to simultaneously achieve desired values of d and $k3$:

- *First filtering for d*: Retain compositions predicted to achieve the desired density within a specified tolerance range.
- *Second filtering for k3*: From the density-filtered dataset, retain compositions predicted to achieve the desired $k3$ within a specified tolerance range.
- *Validation*: Experimentally validate the predicted compositions and refine the model iteratively.

Only $k3$ was chosen for the sequential inverse design because the corresponding foams still exhibit low thermal conductivity under this condition, making them highly suitable for battery-based applications. Additionally, focusing on a single target property ($k3$) simplifies the optimization process, as incorporating a larger number of target properties (e.g., d, $k1$, $k2$ and $k3$) would likely decrease the accuracy and efficiency of the sequential approach.

The general overview of all the experiments conducted in this study, based on different ML methods such as AL and BO, is shown in Figure 1. The initial dataset consists of 23 data points, which served as the foundation for generating ML-driven suggestions. These suggestions were iteratively refined through a combination of experimental validation and computational modeling, ultimately guiding the exploration of the material design space. The final goal of these efforts is the inverse design of experiments, which are located inside the gray regions in Figure 1. These regions represent the most promising areas of the design space, as identified by the ML algorithms.

Most of the inverse designs were performed to achieve desired (arbitrary) values of the density (d), which is a critical parameter for foam performance in battery applications. However, the last four inverse designs (experiments # 96–99) were carried out with the dual objective of achieving specific values for both d and $k3$. This was accomplished using the sequential approach described above, which leverages the predictive power of ML models to iteratively refine the material composition and structure. The success of these experiments demonstrates the effectiveness of the sequential inverse design framework in suggesting experiments exhibiting desired values of different targets simultaneously,

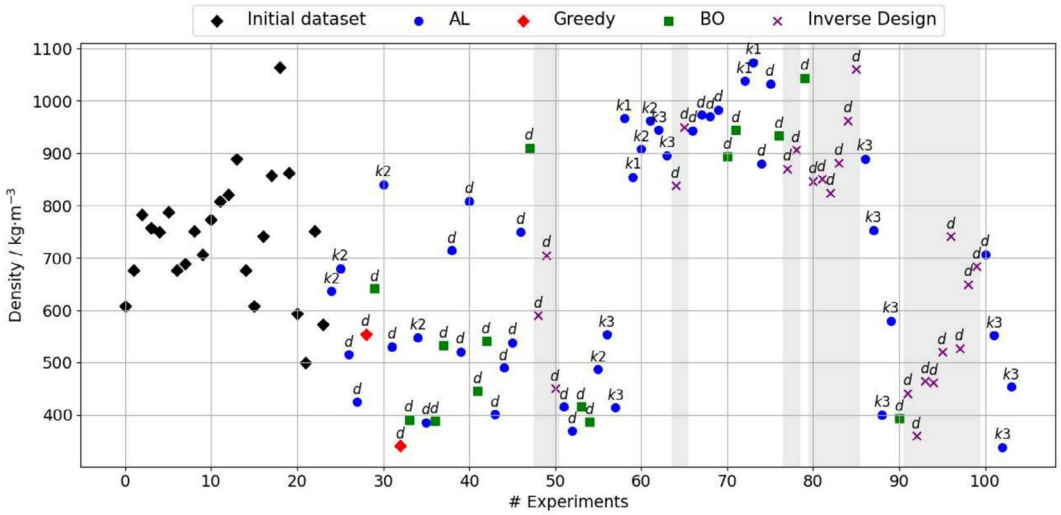

FIGURE 1 | General overview of all the ML-suggested experiments. The first ML suggestions were made using the initial dataset via different strategies like AL, and BO with a final goal of performing inverse design of experiments (points falling on the gray regions). The last 4 inverse designs (experiments # 96–99) were performed aiming at achieving desired *d* and *k3* values (only the *d* label is shown for clarity reasons).

even when dealing with complex and interdependent material properties.

3 | Results and Discussion

Figure 2 shows a typical stress–strain curve (blue line) measured for a representative PUR foam. The force at 10%, 20%, and 30% strain (*k1*, *k2*, and *k3*, respectively), which were used as target properties in this AL investigation, are also shown. The initial experimental dataset comprised of 23 PUR foams with their measured d and $k1 - k3$ targets, as well as their corresponding experimental uncertainties (standard deviations).

This dataset was then used to train initial ML models to suggest new experiments, which was the first step in the AL-ID approach developed in this work, as discussed in the next sections.

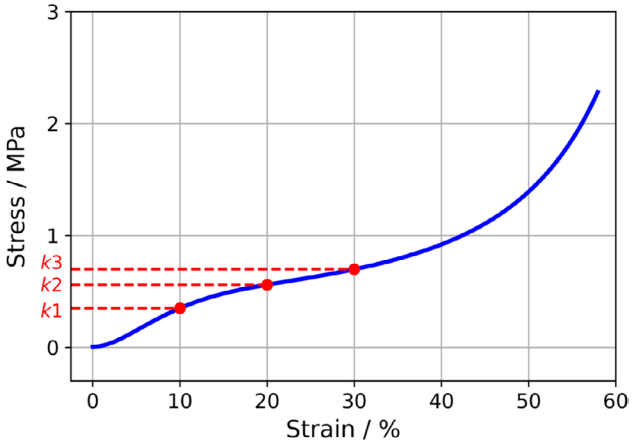

FIGURE 2 | Stress–strain curve for one representative foam of the initial experimental dataset. The target properties *k1*, *k2*, and *k3* are also shown.

3.1 | Evolution of Model Performance With Dataset Growth

To evaluate the impact of dataset size on model performance, we analyzed the evolution of MAE and R^2 score for two key target properties: d and $k3$. The results, presented in Figure 3, demonstrate how the model's predictive accuracy improves as the dataset grows.

ML models rely on data to learn the relationships between input variables and target properties. With a small dataset, the model may struggle to capture these relationships accurately, leading to higher errors and lower predictive power. However, as the dataset grows, the model gains access to more examples, allowing it to better generalize and improve its predictions.

For d, the GBR model demonstrated the best performance, with MAE decreasing and R^2 score increasing as the dataset grew. This indicates that the model became more accurate and reliable with additional data. Similarly, for $k3$, the SVR model outperformed other models, showing a consistent improvement in MAE and R^2 scores as the dataset expanded.

These results highlight the importance of data quantity in developing accurate predictive models. As more experimental data becomes available, the model's predictions become more reliable, enabling better optimization of foam compositions. Additionally, this approach provides a framework for prioritizing experiments: by identifying high-uncertainty regions in the dataset, we can focus experimental efforts on areas that will most improve the model's performance.

3.2 | Evolution of Inverse Design Error With AL Trials

The inverse design process aims to identify optimal foam compositions that achieve specific target properties, such as a desired

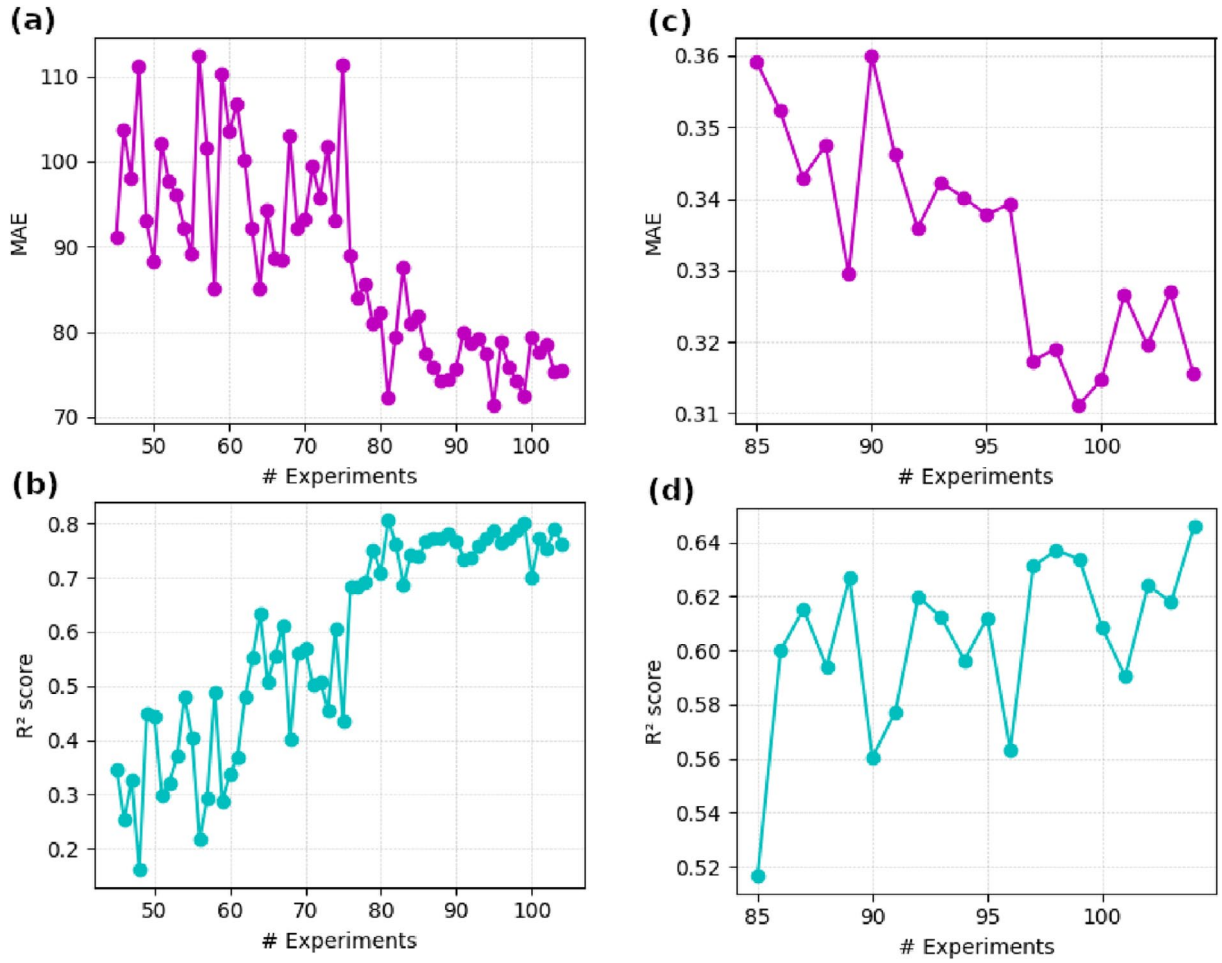

FIGURE 3 | Evolution of model improvement as a function of the number of experiments. Model/target: GBR/d (a, b); SVR/k^3 (c, d). MAE and R^2 are highlighted in purple and turquoise, respectively, to facilitate comparison.

d. To evaluate the effectiveness of this process, we analyzed the evolution of inverse design error as the dataset grew. The results, presented in Figure 4, demonstrate how the error between predicted and actual d values decreases with increasing dataset size, highlighting the model's improving accuracy with the AL trials.

The gray bars represent the error for each inverse design prediction, which corresponds to the gray highlighted areas in Figure 1. At the end, as seen in the figure, the ML-suggested experiments achieve the desired target d with minimal errors. This demonstrates the model's ability to accurately predict optimal foam compositions once it has been trained on a sufficiently large and diverse dataset.

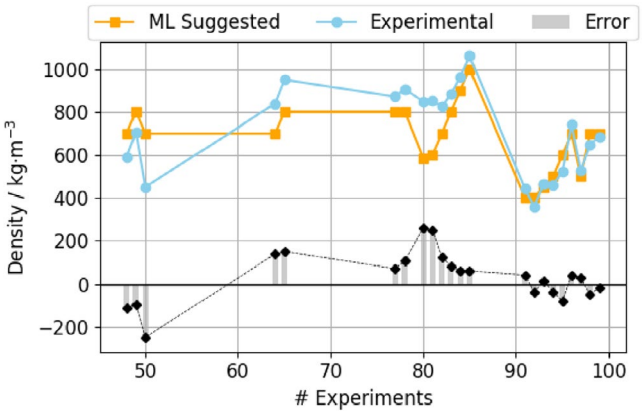

FIGURE 4 | Evolution of Inverse design error of d as the dataset grows. As more AL trials are performed with respect to d, the model becomes more informed in this regard, thereby becoming more accurate in the inverse design process.

3.3 | Parity Plots for Target Properties

To evaluate the predictive accuracy of the best-performing models for each target property, we compared the measured and predicted target properties (d and $k3$) in the so-called parity plots (Figure 5). The predictions were performed after 4-fold CV using the best ML models for d (GBR) and for $k3$ (SVR). In the 4-fold CV setup, each experiment (or point in Figure 5) belonging to one of the four folds was therefore predicted after training a model using all experiments from the three other folds (or 75% of the data). When experimental (or actual) and predicted targets are highly correlated, the corresponding parity plot exhibits higher R^2 scores, indicating that the model performs well. The parity plots shown in Figure 5 reveal that actual and predicted values are well correlated. The R^2 coefficient is better in

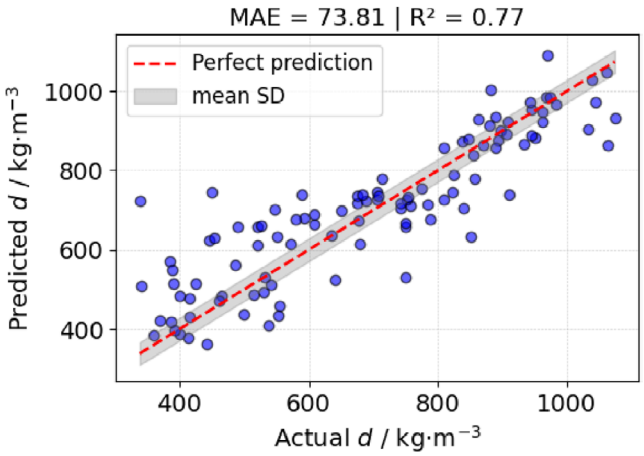

(a) Parity plot for d with GBR model.

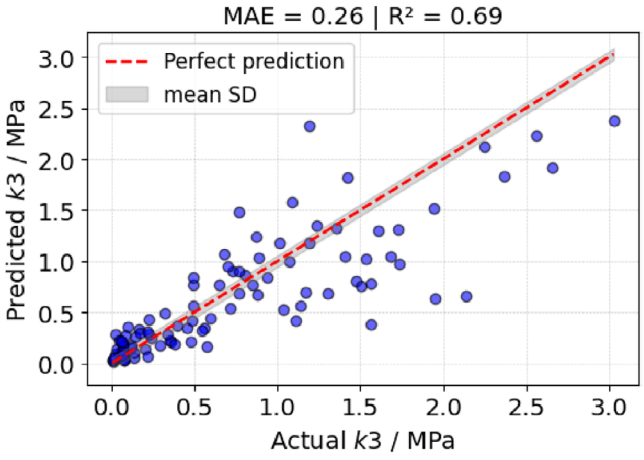

(b) Parity plot for $k3$ with SVR model.

FIGURE 5 | Parity plots for d and $k3$ comparing the experimental and predicted targets. The gray regions represent the mean experimental standard deviations. Five-fold cross validation was used.

Figure 5a compared with Figure 5b, as most AL-based experimental suggestions were based on the improvement of the model for predicting d (compare the total number of d and $k3$ labels in Figure 1). In general terms, these parity plots provide a visual assessment of the accuracy of the model.

As usual, more experiments beyond the 103 experiments carried out in this investigation are expected to improve the model's accuracies, but the sustainable benefits of AL techniques for the efficient development of new materials shall already be clear from the current results.

The GBR model demonstrated good predictive performance for d, with data points closely aligned with the ideal parity line (where predicted values equal actual values). Similarly, the SVR model showed decent predictive performance for $k3$, with most data points following the ideal parity line closely. The R^2 score and MAE, calculated using four-fold cross-validation, confirm the accuracy and reliability of both models.

The use of four-fold cross-validation ensures that the model's performance is robust and not overly dependent on a specific subset of data. These results highlight the potential of ML models to effectively guide experimental efforts by identifying foam compositions that achieve desired target properties with minimal error. The high accuracy of the GBR and SVR models underscores their value in optimizing foam compositions for applications such as EV battery protection.

In addition to the parity plots, an error bar plot was generated to visualize the deviation between actual and predicted values, along with the SD of the experimental data, as is shown in Figure 6. This plot provides a breakdown of the prediction accuracy for individual experiments, highlighting the magnitude of the error and the inherent variability in the data due to experimental conditions. The inclusion of SD information helps contextualize the model's performance, showcasing its ability to make reliable predictions despite experimental noise. This analysis further validates the robustness of the GBR and SVR models in predicting target properties.

3.4 | Inverse Design of Experiments

The sequential filtering approach carried out for all gray vertical regions in Figure 1 is illustrated for one specific case in Figure 7, for which the current experimental dataset size was already 96. This filtering was applied to identify foam compositions that should achieve the following desired target properties: $d = 700\ \mathrm{kg/m^3}$ and $k3 = 1.2$ MPa. Starting with a virtual dataset of 616,008 potential experiments already satisfying all constraints described in Table 3, successive filterings were applied to select the final virtual experiment. First, d was predicted for the virtual dataset using the GBR model, whose distribution is shown in Figure 7a. Figure 7b depicts the virtual compositions whose predictions were in the range $d = 699 - 701\ \mathrm{kg/m^3}$. This initial filtering reduced the dataset from 616,008 to 2597 potential experiments, significantly narrowing the experimental search space.

Next, $k3$ was predicted for the 2597 selected virtual experiments using the SVR model (Figure 7c). Predicted $k3$ values were compared against the desired target range, and virtual experiments falling outside this range were excluded. This second filtering step further reduced the virtual dataset to just 11 virtual experiments (Figure 7d), each predicted to meet both the d and $k3$ requirements. Finally, one virtual experiment out of these 11 was chosen based on the experimental experience of the operator (highlighted by a star in Figure 7d) to be prepared and measured, from where the experimentally measured targets were $d = 742\ \mathrm{kg\,m^{-3}} \pm 24$ and $k3 = 1.19$ MPa ± 0.12. The desired (theoretical) values of $d = 700\ \mathrm{kg\,m^{-3}}$ and $k3 = 1.2$ MPa were in excellent agreement with the measurements, especially after considering the uncertainty of the experiment.

This approach illustrates an efficient strategy for inverse design, enabling the identification of optimal compositions with minimal experimental effort. By focusing only on compositions that meet all target property requirements, as well as the initial compositional restrictions, the approach ensures efficient resource allocation for experimental synthesis and testing.

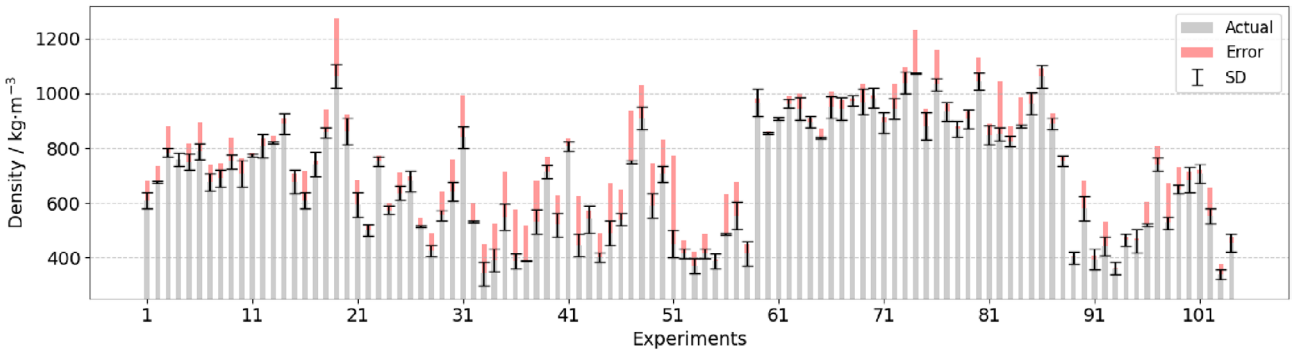

(a) Error distribution for the prediction of d. Model: GBR (4-fold CV).

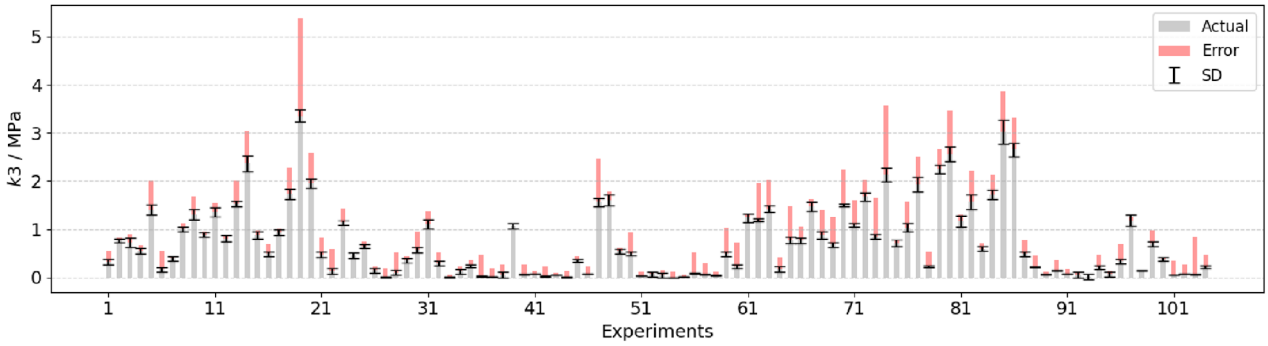

(b) Error distribution for the prediction of $k3$. Model: SVR (4-fold CV).

FIGURE 6 | Error distributions (|actual—predicted|, red vertical bars) for the prediction of (a) d and (b) $k3$. The black vertical error bars are the individual experimental standard deviations.

4 | Final Remarks

It is important to distinguish our approach from multi-objective optimization methods. Our sequential filtering strategy targets specific property ranges by sequentially using different ML models rather than simultaneously optimizing multiple objectives. The Bayesian optimization component was employed solely to explore extreme density values, enhancing dataset diversity for improved model performance. Meanwhile, AL was utilized for other properties to further diversify the dataset. This combination of techniques allowed us to systematically navigate the complex materials space toward compounds with our desired property profiles without requiring the mathematical complexity of a true multi-objective optimization framework.

In our adaptive learning framework, new experimental conditions were selected based on predictive uncertainty from the GP models, focusing on regions where the model had low confidence. By targeting these high-uncertainty areas, we maximized the informational value of each experiment. To address multiple objectives like density and mechanical strength, we alternated focus between them in successive iterations. This simple yet effective strategy allowed balanced progress across both targets without relying on complex multi-objective acquisition functions, which are often unreliable with limited data.

The selection of ML models was guided by the specific requirements of each task in our workflow. GP was used during the AL phase to suggest new experiments, as its ability to quantify predictive uncertainty made it ideal for identifying informative samples. In the end, we also evaluated additional models, from which the best ones were selected, including SVR, GBR, and RF based on their predictive accuracy for each target property. This evaluation was conducted using cross-validated performance metrics such as MAE and R^2. For the inverse design step, we selected the best-performing model for each target. As a result, SVR and GBR were chosen in cases where they outperformed GP. The final sequential filtering has led to a successful inverse design, where desired and experimental targets were in close agreement, as shown in Figure 7.

5 | Conclusion

This study demonstrated the effectiveness of a machine learning-driven framework for the inverse design of PUR foams, particularly for applications like EV battery protection. The sequential combination of the GBR and SVR models for predicting d and $k3$, respectively, has revealed to be an excellent strategy to suggest new experiments simultaneously exhibiting two desired target properties. The final model accuracy shown in the parity plots was already appropriate to allow for a very efficient sequential inverse design, where both measured target properties were in excellent agreement with the desired ones. By integrating virtual data generation, AL, and probabilistic modeling, we efficiently explored the compositional space and identified optimal foam formulations with minimal experimental effort.

While the framework successfully identified optimal foam compositions, certain challenges remain in multi-target

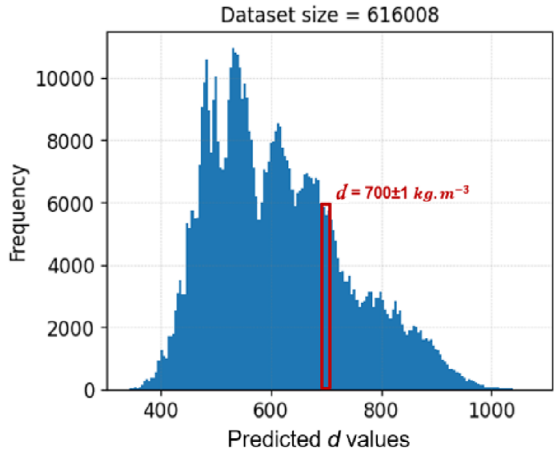

(a) Distribution of d predicted for the virtual dataset using the first trained model.

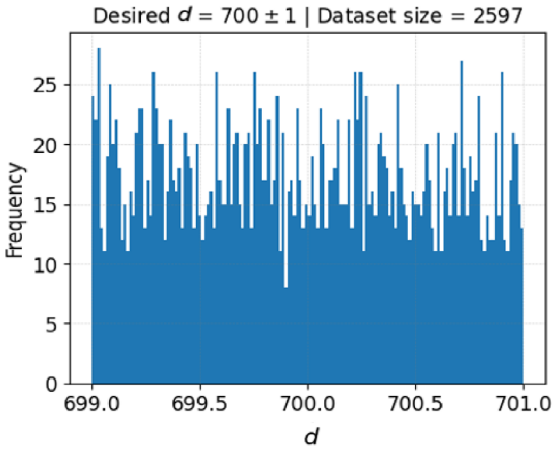

(b) Distribution of predicted d values for the virtual experiments selected inside the red rectangle shown in (a).

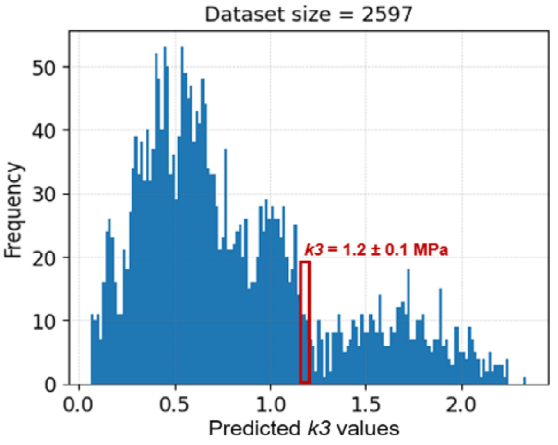

(c) Distribution of $k3$ values predicted using the second trained model for the filtered dataset shown in (b).

(d) Distribution of predicted $k3$ for the virtual experiments selected inside the red rectangle shown in (c).

FIGURE 7 | Sequential filtering approach used in the inverse design to achieve desired d and $k3$ values. Starting with a virtual dataset of 616,008 potential experiments (a), only 2597 of them had the desired predicted d values (b). The distribution of the predicted $k3$ values for these selected virtual experiments (c) was used in the next filtering to find the best candidates exhibiting desired $k3$ values (d). The star highlights the final virtual experiment chosen.

optimization. When AL suggests experiments for different targets at various stages, it can lead to fluctuations in uncertainty estimation, potentially reducing prediction reliability. Additionally, the sequential filtering approach, though effective in narrowing the search space, is influenced by the sensitivity of multiple models applied in succession. Any inaccuracies in the initial predictions can propagate through the filtering steps, impacting the final selection of formulations. Careful management of these factors is crucial to maintaining robustness in the inverse design process.

Future work will explore the integration of physics-informed ML models incorporating domain knowledge about material behavior to improve predictive accuracy and model interpretability. Different AL strategies can also be incorporated to improve the current approach. Additionally, expanding this framework to broader material systems and incorporating additional performance metrics could enhance its generalizability. By bridging computational modeling with experimental validation, this methodology offers a scalable and efficient strategy for designing high-performance polymeric materials.

Acknowledgments

This publication received funding from the University of Bayreuth through the Open Access Publishing funding program. Portions of this research were also supported by the "Bayerischen Staatsministerium für Wissenschaft und Kunst" under grant number F.2-M7426.10.2.1/4/16 in Germany, as well as by the DFG project number 437872031 (AL474/45-1) and by the AUDI AG. We extend our sincere gratitude for the financial support provided.

References

1. IEA, et al., "Global ev Outlook 2020," 2020, https://www.iea.org/reports/global-ev-outlook-2020.

2. A. Yadav, F. M. de Souza, T. Dawsey, and R. K. Gupta, "Recent Advancements in Flame-Retardant Polyurethane Foams: A

Review," *Industrial & Engineering Chemistry Research* 61, no. 41 (2022): 15046–15065.

3. M. Ates, S. Karadag, A. A. Eker, and B. Eker, "Polyurethane Foam Materials and Their Industrial Applications," *Polymer International* 71, no. 10 (2022): 1157–1163.

4. C. Bernardi, B. Toury, M. Salvia, et al., "Effects of Flaming on Polypropylene Long Glass Fiber Composites for Automotive Bonding Applications With Polyurethane," *International Journal of Adhesion and Adhesives* 113 (2022): 103033.

5. C. Alkan, E. Günther, S. Hiebler, Ö. F. Ensari, and D. Kahraman, "Polyurethanes as Solid–Solid Phase Change Materials for Thermal Energy Storage," *Solar Energy* 86, no. 6 (2012): 1761–1769.

6. G. Oertel and L. Abele, *Polyurethane Handbook: Chemistry, Raw Materials, Processing, Application, Properties* (Hanser, 1994).

7. V. Müller, *Investigation of the Influence of Mechanical Pressure on the Aging and the Expansion of Silicon-Containing Lithium-Ion Batteries* (Universitaet Bayreuth, 2020).

8. X. Liu, Z. Ge, W. Zhang, and Y. Luo, "Preparation and Properties of Polyurethane Coatings Modified by Polysilazane," *High Performance Polymers* 32, no. 6 (2020): 611–619.

9. M. P. D. Bauer, D. D. Decker, F. D. Richter, and M. D. Gwiazda, "Hybridpolymere aus cyanaten und silazanen, verfahren zur ihrer herstellung sowie deren verwendung," 2010.

10. S. Steffen, M. Bauer, D. Decker, and F. Richter, "Fire-Retardant Hybrid Thermosetting Resins From Unsaturated Polyesters and Polysilazanes," *Journal of Applied Polymer Science* 131, no. 12 (2014): 40375: 1–7.

11. Y. Liu, C. Niu, Z. Wang, et al., "Machine Learning in Materials Genome Initiative: A Review," *Journal of Materials Science and Technology* 57 (2020): 113–122.

12. C. Lv, X. Zhou, L. Zhong, et al., "Machine Learning: An Advanced Platform for Materials Development and State Prediction in Lithium-Ion Batteries," *Advanced Materials* 34, no. 25 (2022): 2101474.

13. S. M. Pai, K. A. Shah, S. Sunder, R. Q. Albuquerque, C. Brütting, and H. Ruckdäschel, "Machine Learning Applied to the Design and Optimization of Polymeric Materials: A Review," *Next Materials* 7 (2025): 100449.

14. T. Schuett, P. Endres, T. Standau, et al., "Application of Digital Methods in Polymer Science and Engineering," *Advanced Functional Materials* 34, no. 8 (2024): 2309844.

15. F. L. Lee, J. Park, S. Goyal, et al., "Comparison of Machine Learning Methods Towards Developing Interpretable Polyamide Property Prediction," *Polymers* 13, no. 21 (2021): 3653.

16. Z. Heidari and M. A. Sobati, "Evaluation of the Flammability Characteristics of Alkyl Esters: New Qspr Models," *Journal of Molecular Liquids* 387 (2023): 122697.

17. K. A. Shah, R. Q. Albuquerque, C. Brütting, M. Dippold, and H. Ruckdäschel, "Low-Density Polyamide 12 Foams Using Bayesian Optimization and Inverse Design," *Polymer* 320 (2025): 128096.

18. E. Kazemi-Khasragh, J. P. Fernández Blázquez, D. Garoz Gómez, C. González, and M. Haranczyk, "Facilitating Polymer Property Prediction With Machine Learning and Group Interaction Modelling Methods," *International Journal of Solids and Structures* 286 (2024): 112547.

19. R. Bhowmik, S. Sihn, R. Pachter, and J. P. Vernon, "Prediction of the Specific Heat of Polymers From Experimental Data and Machine Learning Methods," *Polymer* 220 (2021): 123558.

20. R. Q. Albuquerque, F. Rothenhäusler, P. Gröbel, and H. Ruckdäschel, "Multi-Objective Optimization of Sustainable Epoxy Resin Systems Through Bayesian Optimization and Machine Learning," *ACS Applied Engineering Materials* 1, no. 12 (2023): 3298–3308.

21. P. Endres, T. Schuett, C. Brütting, et al., "Systematic Copolymer Screening for Foaming Experiments Supported by Computational Methods," *Journal of Materials Chemistry A* 11, no. 47 (2023): 26183–26192.

22. J. R. Deneault, J. Chang, J. Myung, et al., "Toward Autonomous Additive Manufacturing: Bayesian Optimization on a 3d Printer," *MRS Bulletin* 46 (2021): 566–575.

23. F. Omoruwou, A. A. Ojugo, and S. E. Ilodigwe, "Strategic Feature Selection for Enhanced Scorch Prediction in Flexible Polyurethane Foam Manufacturing," *Journal of Computing Theories and Applications* 1, no. 3 (2024): 346–357.

24. A. Admasu, D. Upadhyay, R. Couvreur, J. Tardiff, A. Kiziltas, and P. Blanchard, "Deep Learning Image-Based Design of Graphene-Reinforced Polyurethane Foams," 2022.

25. H. Ergün and M. E. Ergün, "Modeling Xanthan Gum Foam's Material Properties Using Machine Learning Methods," *Polymers* 16, no. 6 (2024): 740.

26. F. Chevillotte, "Porous Material Characterization With Bayesian and Machine Learning Method," in *INTER-NOISE and NOISE-CON Congress and Conference Proceedings*, vol. 270 (Institute of Noise Control Engineering, 2024), 9590–9597.

27. P. Sharma and V. R. P. Kumar, "Prediction and Analysis of Sandwich Panel With Rice Husk and Polyurethane Foam Using Machine Learning Model," *Asian Journal of Civil Engineering* 24, no. 8 (2023): 3009–3021.

28. J. A. Pugar, "Multiscale Modeling of Polyurethane Properties via Latent Variables with Hierarchical Machine Learning. PhD thesis, Carnegie Mellon University," 2023.

Supporting Information

Additional supporting information can be found online in the Supporting Information section.